INTERNATIONAL JOURNAL FOR NUMERICAL METHODS IN FLUIDS
Int. J. Numer. Meth. Fluids 2007; **53**:777–792
Published online 5 October 2006 in Wiley InterScience (www.interscience.wiley.com). DOI: 10.1002/fld.1306

Adaptive Euler simulations of airfoil–vortex interaction[§]

Lei Tang[1,*,†] and James D. Baeder[2,‡]

[1]*ZONA Technology, Inc., Scottsdale, Arizona 85258, U.S.A.*
[2]*Department of Aerospace Engineering, University of Maryland, College Park, Maryland 20742, U.S.A.*

SUMMARY

A grid redistribution method is used together with an improved spatially third-order accurate Euler solver to improve the accuracy of direct Euler simulations of airfoil–vortex interaction. The presented numerical results of two airfoil–vortex interaction cases indicate that with combination of the two methods, the numerical diffusion of vorticity inherent in the direct Euler simulations is drastically reduced without increasing the number of grid points. With some extra works due to grid redistribution, the predicted vortex structure is well preserved after a long convection and much sharper acoustic wave front resulting from airfoil–vortex interaction is captured. Copyright © 2006 John Wiley & Sons, Ltd.

Received 16 November 2005; Revised 16 June 2006; Accepted 16 June 2006

KEY WORDS: grid redistribution; vortex preservation; shock–vortex interaction; airfoil–vortex interaction; geometry conservation law

1. INTRODUCTION

Despite rapid progresses of computational fluid dynamics (CFD) techniques, the accurate Euler/Navier–Stokes simulation of supercritical interaction of airfoil and vortex still remains one of the most challenging problems for CFD. This is because for this case, a numerical method is required to not only correctly capture strong shocks but also accurately preserve the vortex structure before the vortex passes by the trailing edge of the airfoil. However, it is a common experience that the predicted vortex structure is diffused very rapidly as the vortex convects in the flowfield due to large numerical diffusion contained in upwind shock-capturing schemes and

*Correspondence to: Lei Tang, UARC/AFDD, NASA Ames Research Center, M/S 215-1, Bldg 215, Moffett Field, CA 94035, U.S.A.
†E-mail: ltang@merlin.arc.nasa.gov
‡E-mail: baeder@eng.umd.edu
§Presented as AIAA-03-3826.

Contract/grant sponsor: National Rotorcraft Technology Center (NRTC)
Contract/grant sponsor: NSF; contract/grant number: DMI-0232255

insufficient grid resolution in the vortex region. As a result, the effect of airfoil–vortex interaction is significantly underpredicted. Some prescribed vortex approaches, such as the perturbation method [1], the surface transpiration method [2], and the field velocity approach [3], have been adopted in practice.

Recently, research has been conducted towards reduction of the numerical diffusion of vorticity contained in direct Euler/Navier–Stokes simulation. The vorticity confinement method of Steinhoff *et al.* [4], similar to a central scheme with artificial viscosity, introduces an extra confinement term for controlling the size of the vortex structure. The accurate determination of this confinement term, however, is problem dependent. It is more natural and robust to reduce the numerical diffusion of vorticity by improving the accuracy of numerical discretization and grid resolution in the vortex region.

A popular approach for the accuracy improvement of numerical discretization is to use a higher-order spatial discretization. For example, a fifth-order polynomial fit of the interface values has been suggested to replace the more traditional third-order one used in the famous MUSCL scheme for better preservation of the vortex structure [5–7]. In fact, this fifth-order polynomial fit of the interface values has also been used in many advanced monotone schemes (e.g. References [8, 9]) for the smooth regions to achieve higher accuracy over the MUSCL approach. However, recent numerical analysis and results have exposed a contradiction between the order of accuracy and the spectral resolution capability of a numerical scheme (e.g. References [10–12]). Especially it has been shown in References [13, 14] that an improved third-order accurate upwind spatial discretization, a piecewise quadratic reconstruction with the sixth-order compact difference computed slope and curvature, is much less diffusive than the above fifth-order spatial discretization.

As for enhancement of the grid resolution in the vortex region, both multiblock grids [5] and local refinement method [15–17] have been investigated before. On the other hand, the simplest and most cost-effective method for grid resolution enhancement, grid redistribution, has not been explored for direct Euler/Navier–Stokes simulation of airfoil–vortex interaction. This is probably because as pointed out in Reference [18], most grid redistribution methods are unable to produce large grid adaptation.

In this paper, the two-step grid redistribution method of Reference [19] will be used together with the improved spatially third-order accurate Euler solver of Reference [14] to achieve accurate Euler simulations of two airfoil–vortex interaction cases, one is a subcritical head-on interaction and the other is a supercritical interaction. The accuracy of the direct Euler simulations will be validated with the experimental data in Reference [20] and a prescribed vortex approach like the perturbation method in Reference [1].

2. COMPUTATIONAL GRID

The airfoil in the two selected interaction cases is NACA0012. Figure 1 presents the baseline C-grid around the airfoil generated using a hyperbolic grid generator. There are 217 grid points in the wraparound (along the chord) direction with 144 points on the body, and 151 points in the normal direction. The grid is clustered near the leading and trailing edges (also the shock positions in the supercritical case). The first grid spacing from the surface in the normal direction is 0.001 chords. The outer boundaries of the grid are extended to 20 chords in all directions.

This baseline C-grid, as shown in Figure 1, has good resolution only around the airfoil. If a vortex is not close to the airfoil, it is very likely, depending on the exact location of the vortex, to

DOI: 10.1002/fld

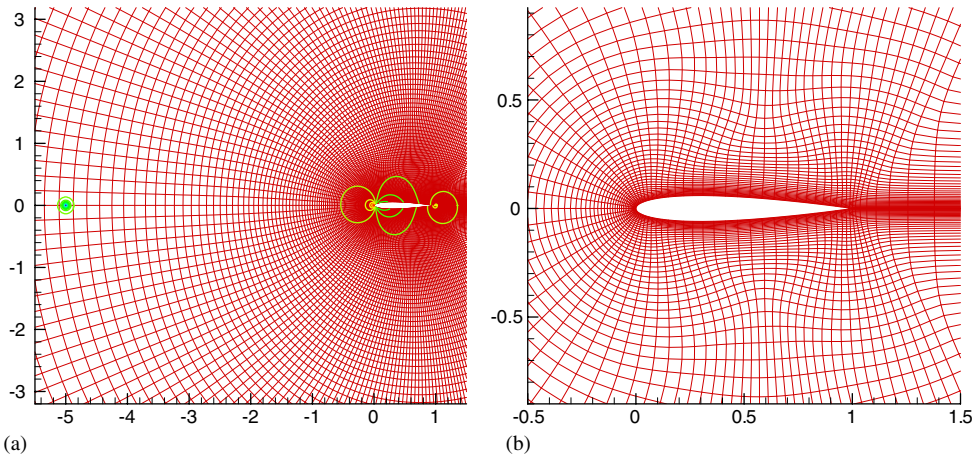

Figure 1. Baseline C-grid: (a) global view including both airfoil and vortex; and (b) blow-up near the airfoil (every other points).

have no grid points or only one or two across the vortex core. In order to accurately capture or preserve this vortex structure, the two-step grid redistribution method of Reference [19] will be used to locally refine this grid in the vortex region.

Instead of direct application of a grid redistribution method to adapt the baseline C-grid in the physical domain, this two-step procedure uses an elliptic grid redistribution method of Reference [21] to adapt the indices of the baseline grid in the computational domain in the first step. With these new indices, a cubic interpolation is used in the second step to further move the grid points of the baseline C-grid in the physical domain. As shown in Figure 2, such an approach can achieve much larger grid adaptation than a single-step elliptic grid redistribution method whereas the robustness of an elliptic grid redistribution method is preserved. If the distortion of the grid were not concerned, the grid adaptation provided by this two-step procedure would have no limit since no grid line crossover would happen. This can be achieved by multiple uses of the second interpolation step. In practice, of course, the maximum grid redistribution is restricted by the allowable grid distortion and the convergence of computation. The detail of this two-step grid redistribution method is referred to Reference [19].

This two-step grid redistribution method controls the grid spacing by the length scale l. The smaller the local l is, the more the grid refinement will be achieved. For the following two airfoil–vortex interaction cases, the length scale l is determined by a modified point attraction function, in which l depends on r, the distance of a grid point from the vortex centre

$$l = \begin{cases} 1 - A, & r \leqslant R_1 \\ 1 - A + A\left(3 - 2\dfrac{r - R_1}{R_2 - R_1}\right)\left(\dfrac{r - R_1}{R_2 - R_1}\right)^2, & R_1 < r < R_2 \\ 1, & r \geqslant R_2 \end{cases} \tag{1}$$

DOI: 10.1002/fld

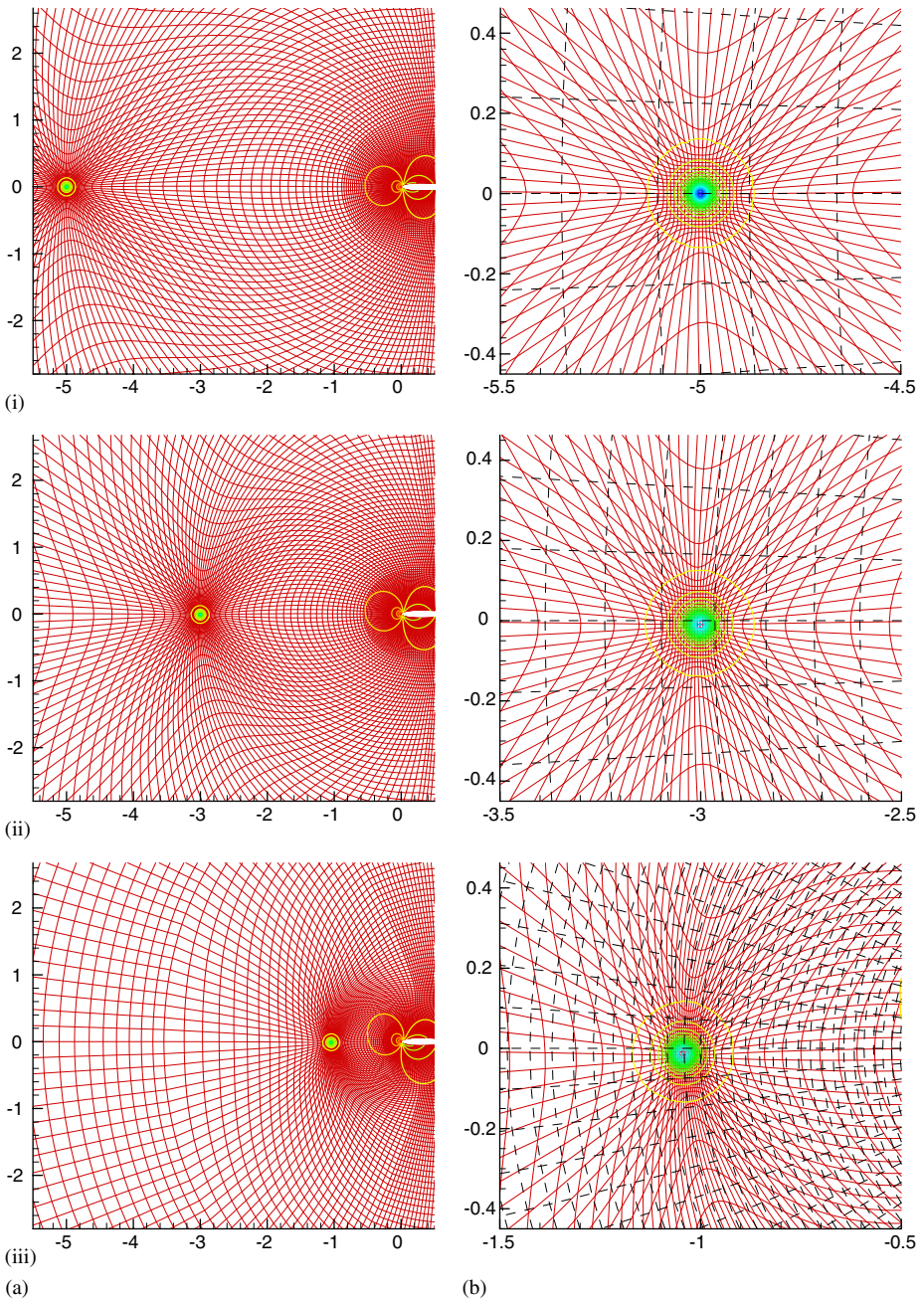

Figure 2. Adapted grids and the predicted vortex structure for the subcritical head-on interaction: (i) $t=-5$; (ii) $t=-3$; and (iii) $t=-1$. (a) Global view including both airfoil and vortex; and (b) blow-up around the vortex region (black dash line—baseline grid).

DOI: 10.1002/fld

Here $r \leqslant R_1$ defines the region for local refinement, $r \geqslant R_2$ defines the unadapted region, and $R_1 < r < R_2$ defines the transition region.

It is clear that the parameter A represents the adaptation strength. The closer the value of A is to one, the more adaptation that will be taken. In the following two airfoil–vortex interaction cases, A will vary with the distance of the vortex centre from the leading edge of the airfoil. When the vortex is farther than two chords upstream of the leading edge, A takes its maximum value of 0.98. Then the value of A decreases as the vortex approaches to the airfoil. After the vortex attains 0.05 chords upstream of the leading edge, the value of A is set to zero. This is because the resolution of the baseline C-grid in the vortex region, as shown in Figure 1, increases when the vortex approaches to the airfoil. More importantly, when the vortex is very close to the airfoil, the implementation of grid redistribution in the vortex region may degrade the high quality of the grid near the airfoil surface. So, we not only turn off the grid redistribution when the vortex is very close to the airfoil but also adjust R_2 based on the value of A to keep the six grid lines adjacent to the airfoil surface in the normal direction as the unadapted region whenever the grid redistribution is implemented. However, the adjustment of R_2 to a small value may lead to a poor grid quality, especially for a drastic grid adaptation. It is our experience that the value of R_2 should be at least 3 or 4 times that of R_1 for the maximum A.

Figure 2 presents the adapted grids at the three selected time steps. When the vortex is 5 chords upstream of the leading edge of the airfoil, the adapted grid is found to have about 24 cells within one cell of the baseline grid in the vortex region. Such a grid refinement is usually not achievable by an elliptic grid redistribution method. Even a local refinement method requires more than four levels of subdivisions, which would increase the local computational effort by 24×24 times. On the other hand, the extra computational cost due to grid redistribution with $A = 0.98$ is about two times the cost of the flow solver. Furthermore, with decrement of A, this computational overhead associated with grid redistribution can drop by up to one order of magnitude by using over-relaxation instead of under-relaxation scheme to solve the elliptic equations. It is also clear that the grid quality inside the local refinement region is pretty good. However, the grid lines in the transition region are significantly skewed. So, an improvement will be given in the next section for computation of the Jacobian of the coordinate transformation on a significantly distorted grid.

3. NUMERICAL ALGORITHM

The Euler equations are the simplest governing equations which can independently simulate a supercritical interaction between airfoil and vortex. The equations can be written in the conservation form in a generalized body-fitted curvilinear coordinate system as follows:

$$\partial_t \hat{Q} + \partial_\xi \hat{E} + \partial_\eta \hat{F} = 0 \tag{2}$$

where $\hat{Q}$ is the vector of the conservative variables, $\hat{E}$ and $\hat{F}$ are the flux vectors, ξ and η are the curvilinear coordinates. A detailed description of these terms can be found in many references like Reference [13].

The baseline Euler solver used in this study is the Euler mode of Transonic Unsteady Rotor Navier–Stokes (TURNS) code [22], which uses the Lower–Upper Symmetric-Gauss–Seidel (LU-SGS) implicit scheme for the left-hand-side operator to yield good stability and convergence characteristics, along with Roe's upwinding for the right-hand-side operator to significantly

DOI: 10.1002/fld

improve the viscous computation. The option of using Newton-type subiterations at each time step allows for reduction of the linearization and factorization errors and improvement of the time accuracy. A detailed description of the algorithm is referred to References [13, 22].

In the baseline TURNS code, the highest spatial accuracy is achieved by using a third-order polynomial fit of the interface values, which can also be interpreted as a piecewise quadratic reconstruction of the solution with the second-order divided difference computed slope and curvature. Such a flow solver has been found very diffusive for simulation of vortex-dominated flows [6, 7]. To improve the numerical accuracy over this spatial discretization, a more popular approach is to use a higher-order (e.g. fifth-order) polynomial fit of the interface values [5–7]. However, both Fourier accuracy analysis and the numerical result of a simple two-dimensional vortex convection case in References [13, 14] have indicated that it would be much more effective for reduction of numerical diffusion by keeping the piecewise quadratic reconstruction of the solution but with the more accurate sixth-order compact difference computed slope and curvature. The resulting improved third-order accurate spatial discretization is called as Q6c, i.e. piecewise Quadratic reconstruction with sixth-order compact difference computed slope and curvature. As shown in References [13, 14], Q6c can dramatically reduce the numerical decay of the normalized peak-to-peak vertical velocity induced by a vortex after 200 core radii convection predicted by the traditional third-order spatial discretization from 44 to 4% on a coarse mesh with only four points across the vortex core whereas the fifth-order spatial discretization only reduces the numerical decay to 32%. Furthermore, after imposing the monotonicity-preserving constraints, MQ6c (monotonicity-preserving Q6c) is still able to reduce the numerical decay predicted by the third-order MUSCL scheme used in the baseline TURNS code from 46 to 22% whereas WENO5 [8], a monotonicity-preserving fifth-order spatial discretization, only reduces the numerical decay to 37%. Therefore, this improved third-order accurate spatial discretization, MQ6c, will be used in the modified TURNS code to alleviate the grid resolution requirement for accurate Euler simulation of airfoil–vortex interaction.

Another modification made for improving the accuracy of TURNS code is the computation of J, the Jacobian of the coordinate transformation. Originally, the TURNS code uses a popular procedure to compute J, i.e. set J at the point (i, j) equal to the area of the quadrilateral with the centres of four neighbouring cells as the vertices. However, after a large grid adaptation, it is possible for the point (i, j) to stay outside this quadrilateral (see the left one in Figure 3). As a

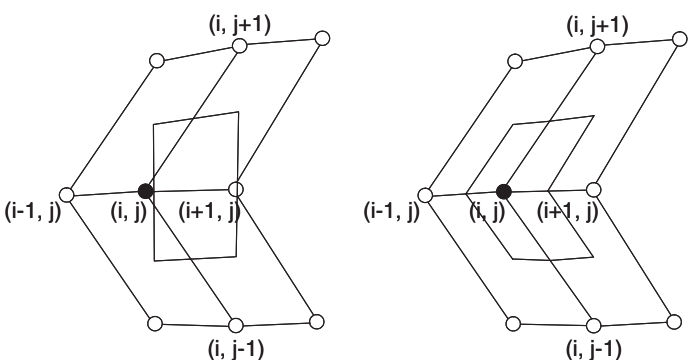

Figure 3. Two types of dual meshes for computation of J.

DOI: 10.1002/fld

result, the computation of J is not accurate. In the modified TURNS code, this quadrilateral is replaced with a polygon with eight sides, each of which connects the centre of a neighbouring cell with the midpoint of the common side (see the right one in Figure 3). Therefore, J is more accurately computed at the cost of twice the computational effort of the quadrilateral.

To account for the effect of a deforming mesh, the so-called geometric conservation law is further enforced in the computation of the time metrics associated with the coordinate transformation. The original approach in Reference [23] is to compute J as follows:

$$\partial_t(J^{-1}) + \partial_\xi(J^{-1}\xi_t) + \partial_\eta(J^{-1}\eta_t) = 0 \tag{3}$$

In practice, however, it is probably simpler to still compute the Jacobian J by its geometric definition but compute the time metrics according to the geometric conservation law [24]

$$\begin{aligned} \frac{\xi_t}{J} &= -\frac{V_{S^\xi}}{\Delta t} \\ \frac{\eta_t}{J} &= -\frac{V_{S^\eta}}{\Delta t} \end{aligned} \tag{4}$$

where V_{S^ξ} and V_{S^η} represent the volume swept by the cell surfaces along the ξ and η directions, respectively.

Figure 4 presents the predicted pressure contours for the subcritical head-on interaction case. It is found that without implementation of geometric conservation law, the obtained solution has some numerical noises radiated from the leading edge of the airfoil and the solution is distorted. On the other hand, after implementation of geometric conservation law, the resulting numerical solution is very clean, indicating the necessity of implementing geometric conservation law for a deforming mesh.

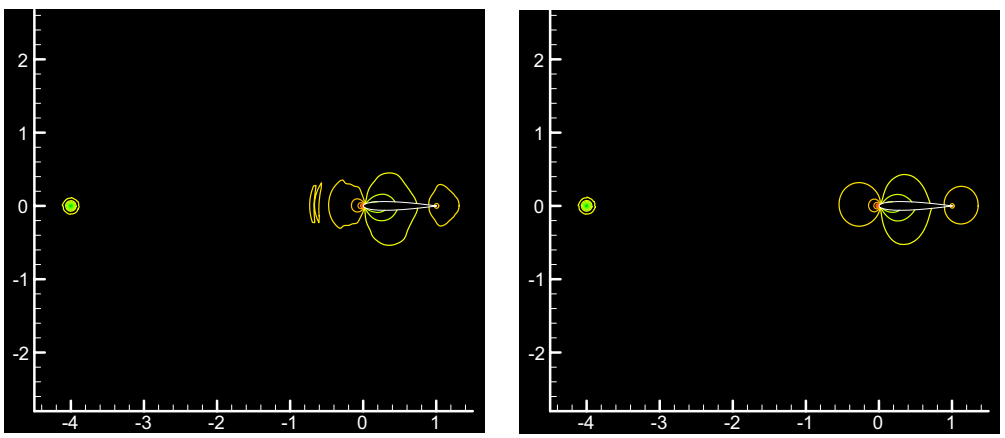

(a) (b)

Figure 4. Pressure contours of subcritical head-on interaction case: (a) without GCL; and (b) with GCL (Min = 0.24, Max = 0.84, Interval = 0.02).

DOI: 10.1002/fld

4. RESULTS AND DISCUSSION

In this section, the results of the direct Euler simulations of two airfoil–vortex interaction cases will be presented. One is a subcritical head-on interaction and the other is a supercritical interaction. In both cases, the airfoil considered is NACA0012 and the vortex structure is Kauffman/Scully type.

4.1. Subcritical head-on interaction

The first case considered here is the subcritical head-on interaction case in Reference [20]. Our objective is to use the experimental data in Reference [20] to verify the significantly reduced numerical diffusion in the direct Euler simulation by combining the two-step grid redistribution method of Reference [19] and the improved spatially third-order accurate Euler solver of Reference [14]. According to Reference [20], the freestream Mach number is 0.5, and the vortex has a non-dimensionalized strength of 0.283 and a core radius of 0.018 chords. This is an extremely tight vortex and imposes a very strict requirement on the local grid resolution in the vortex region.

The C-grid in Figure 1 is used as the baseline grid for the computation. The two-step grid redistribution method of Reference [19] is used to locally refine the mesh in the vortex region. The computation starts with the calculation of the steady solution around the NACA0012 airfoil. This is followed by imposing the vortex on the flowfield 5 chords upstream of the leading edge of the airfoil. After that, the vortex is released and convects downstream using unsteady computation. At each time step, the grid is adapted. The resulting adapted grids have been shown in Figure 2. The second-order backward time discretization is used with the geometric conservation law extended to the second-order backward scheme. This avoids the interpolation of the solutions between two neighbouring deforming meshes. A small Δt of 0.005 with six subiterations is chosen to keep the time accuracy.

The measured time histories of the surface pressure coefficient at three chordwise locations (2, 5, and 10% of the chord length) in Reference [20] are used to verify the reduced numerical diffusion contained in the direct numerical simulation by combining the two-step grid redistribution method of Reference [19] and the improved spatially third-order accurate Euler solver of Reference [14]. It is found in Figure 5 that compared with multiblock grid Navier–Stokes results in Reference [20] based on nearly 193 000 points, our adaptive Euler computation with only about 32 800 points gives much steeper slopes of the pressure and much larger peak values due to much less numerical diffusion inherent in the computation. Since the viscous terms are not included in our computation, the predicted slopes of pressure in the present computation are even slightly steeper than the experimental data.

It is also found that our computational results match the experimental data much better over the upper surface than over the lower surface. Especially a spike exists in each pressure trace on the lower surface. This is because the viscous effect is very important over the lower surface due to the vortex induced separation near the leading edge and the following mix of vortices, as shown in Figure 6. On the other hand, the viscous effect over the upper surface can be neglected. Figure 6 compares the computational density snapshots with the experimental holograms in Reference [20] at the four selected time steps. They look similar but not quantitatively same, indicating the necessity of performing a viscous computation for this case.

The most quantitative measure of numerical diffusion in the computation is probably the predicted induced velocity profile across the vortex, which is difficult to obtain accurately in the

DOI: 10.1002/fld

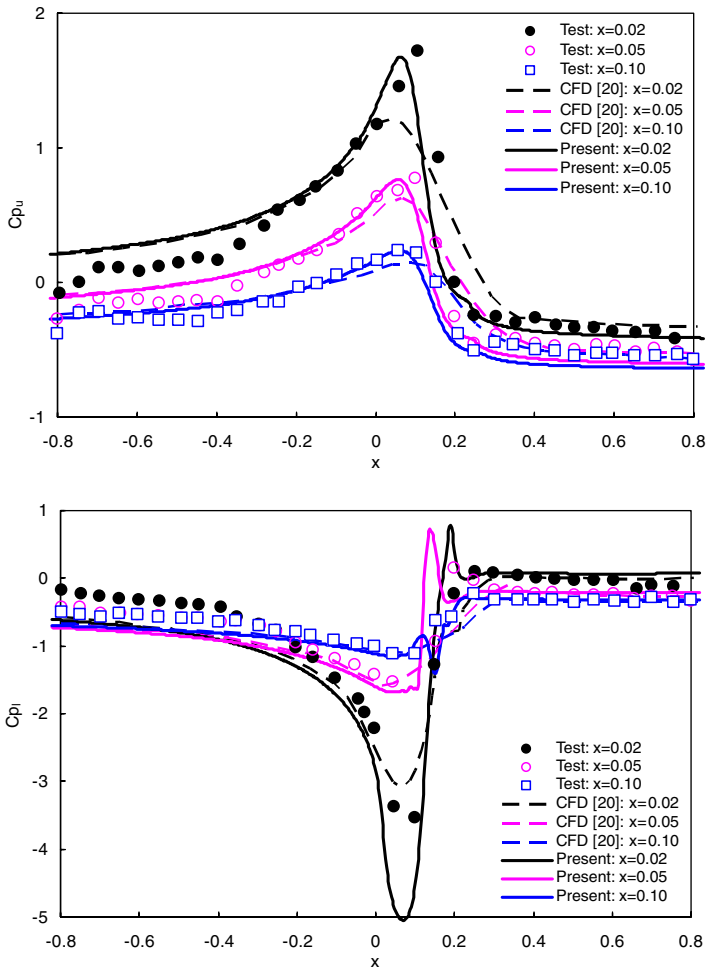

Figure 5. Comparison of computational and experimental pressure histories during subcritical head-on interaction.

context of an airfoil–vortex interaction. This is because there is likely no grid line across the vortex core and the existence of the airfoil causes the induced velocity too. Fortunately in our case, as shown in Figure 2, after grid redistribution, there is always a grid line across the vortex core, which is nearly parallel to the freestream when the vortex is not close to the airfoil. Because the airfoil induced vertical velocity near the line of $y = 0$ is also negligible, the distribution of the vertical velocity along the grid line across the vortex centre can be approximately considered as the vortex induced velocity profile. Figure 7 presents such numerical results when the vortex is $5, 4, 3, 2, 1$ chords upstream of the leading edge of the airfoil. It is found that without grid redistribution and improved numerical discretization, the baseline TURNS methodology predicts a significantly diffused vortex with the initial strength only $\frac{1}{3}$ of the one given by the modified TURNS methodology (also partially because of no grid line across the vortex centre in the baseline

DOI: 10.1002/fld

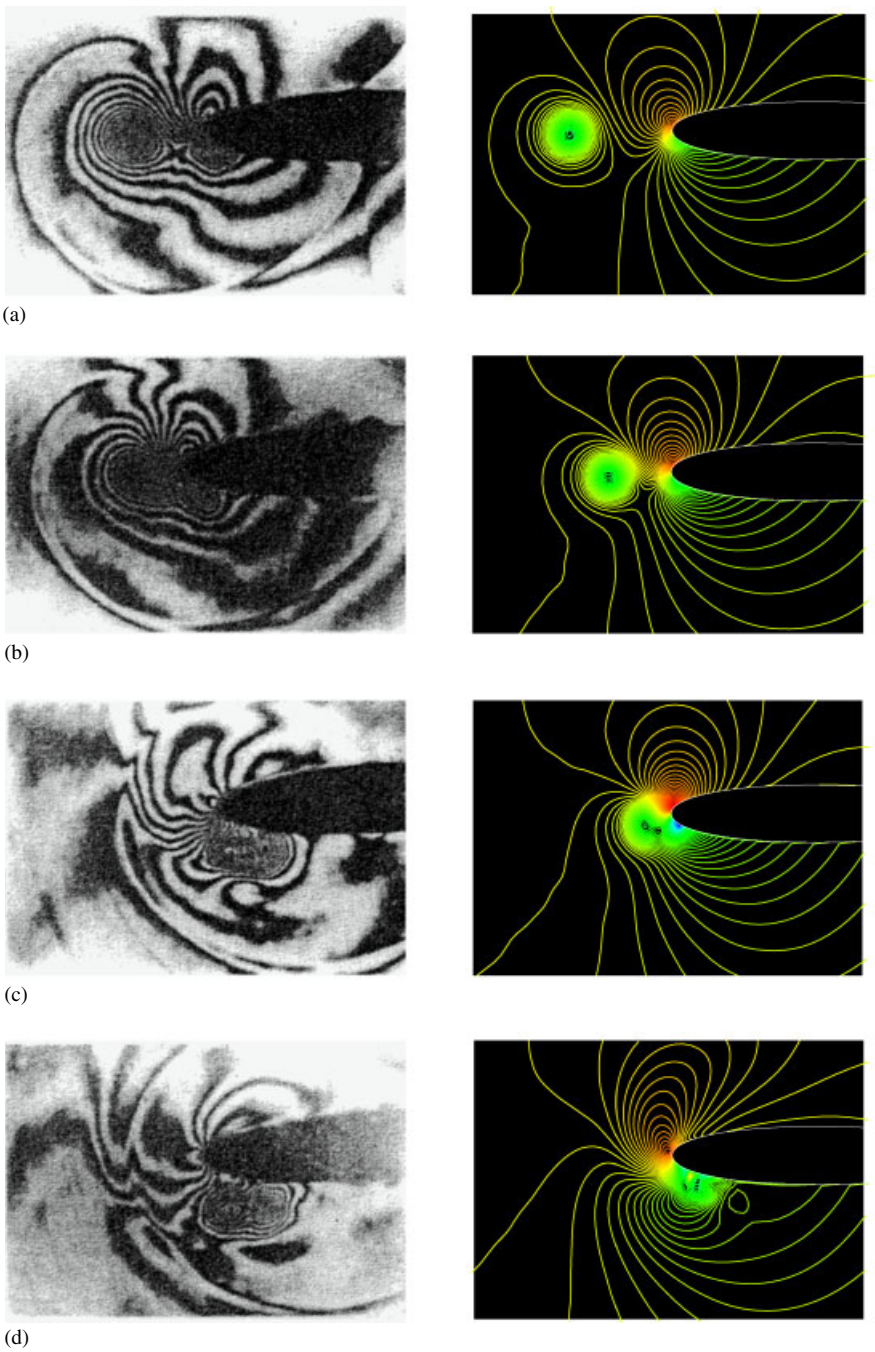

Figure 6. Comparison of experimental holograms and computational snapshots for subcritical head-on interaction: (a) $t = 4.86$; (b) $t = 4.95$; (c) $t = 5.04$; and (d) $t = 5.13$ (density contours: Min $= 0.24$, Max $= 0.84$, Interval $= 0.02$).

DOI: 10.1002/fld

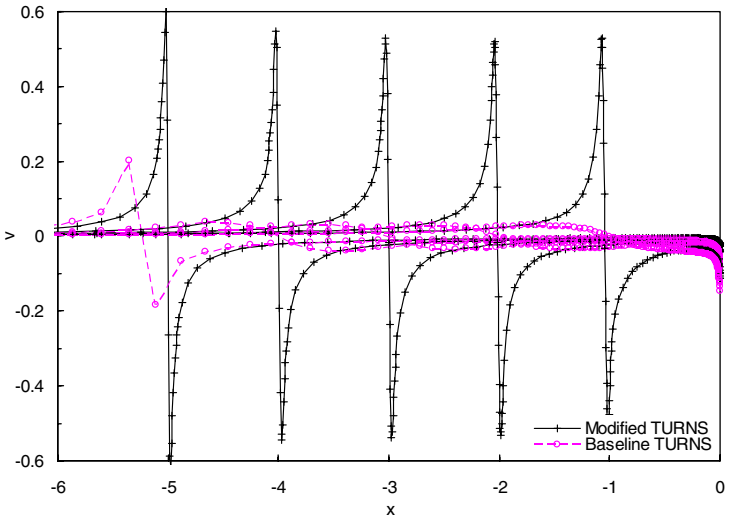

Figure 7. Distributions of vertical velocity across the vortex for subcritical head-on interaction.

C-grid). After a short convection, the stabilized profile only has about 10% of its initial strength. On the other hand, the final vortex profile given by the modified TURNS methodology keeps 90% of the initial strength.

4.2. Supercritical airfoil–vortex interaction

Our major test case is a supercritical interaction between NACA0012 airfoil and the Kauffman/Scully vortex, which has a non-dimensionalized strength of 0.2 and a core radius of 0.05 chords. The freestream Mach number considered is 0.8 under which relatively strong shocks exist over both the upper and lower surfaces of the airfoil even without the vortex. To accurately simulate such an airfoil–vortex interaction, a numerical scheme is required to have not only the shock-capturing capability but also the vortex-preserving capability.

The baseline grid used for the computation is almost the same as the C-grid presented in Figure 1 except the grid clustering around the shock positions. Again, the two-step grid redistribution method of Reference [19] is used to locally refine the mesh in the vortex region. The computation starts with the calculation of the steady solution around the NACA0012 airfoil. This is followed by imposing the vortex on the flowfield 5 chords upstream of the leading edge of the airfoil and one-quarter of a chord below the airfoil. No experimental data is available for this case. But the perturbation method [1] has been well validated for this weak interaction and can be used to examine the accuracy of the direct Euler simulation.

The most basic measure of the airfoil–vortex interaction is the time history of loading during the vortex passage. Figure 8 uses the result of the perturbation method [1] to examine the numerical diffusion inherent in the baseline and modified TURNS methodology. It is found that the baseline TURNS methodology considerably underpredicts the effect of airfoil–vortex interaction. This can be observed in both the magnitude of the negative peak loading as well as the slope of the loading as the vortex passes underneath the airfoil. The combination of the grid redistribution method of

DOI: 10.1002/fld

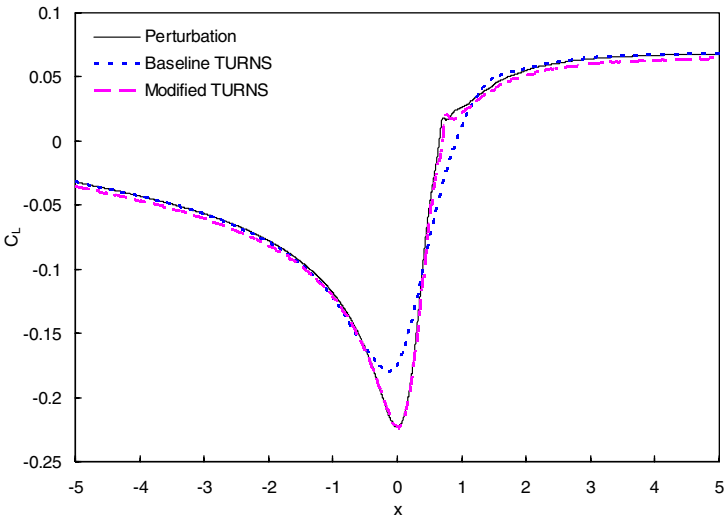

Figure 8. Time history of loading during supercritical airfoil–vortex interaction.

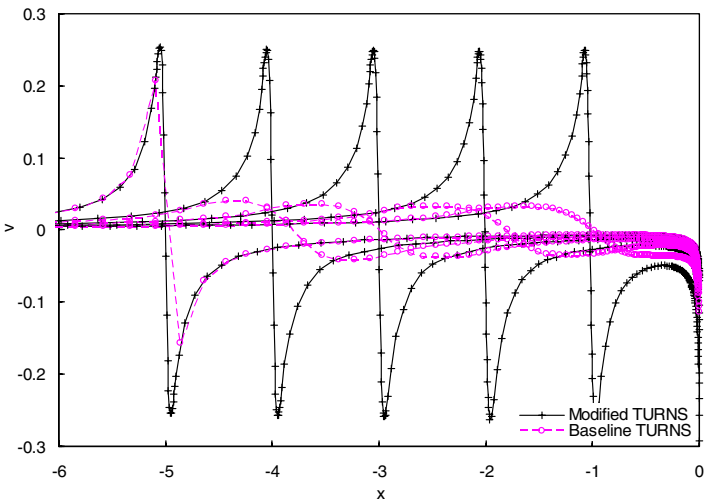

Figure 9. Distributions of vertical velocity across the vortex for supercritical head-on interaction.

Reference [19] and the improved Euler solver of Reference [14] significantly improves the result. In fact, the result from the direct Euler simulation using the modified TURNS methodology is almost identical to the one given by the perturbation method.

The above phenomenon is attributed to the fact that the modified TURNS methodology is able to accurately preserve the vortex structure while the baseline TURNS methodology fails to do that. Figure 9 presents the predicted vortex induced velocity profiles across the vortex core given by the two approaches. It is found that up to one chord upstream of the leading edge of the airfoil,

DOI: 10.1002/fld

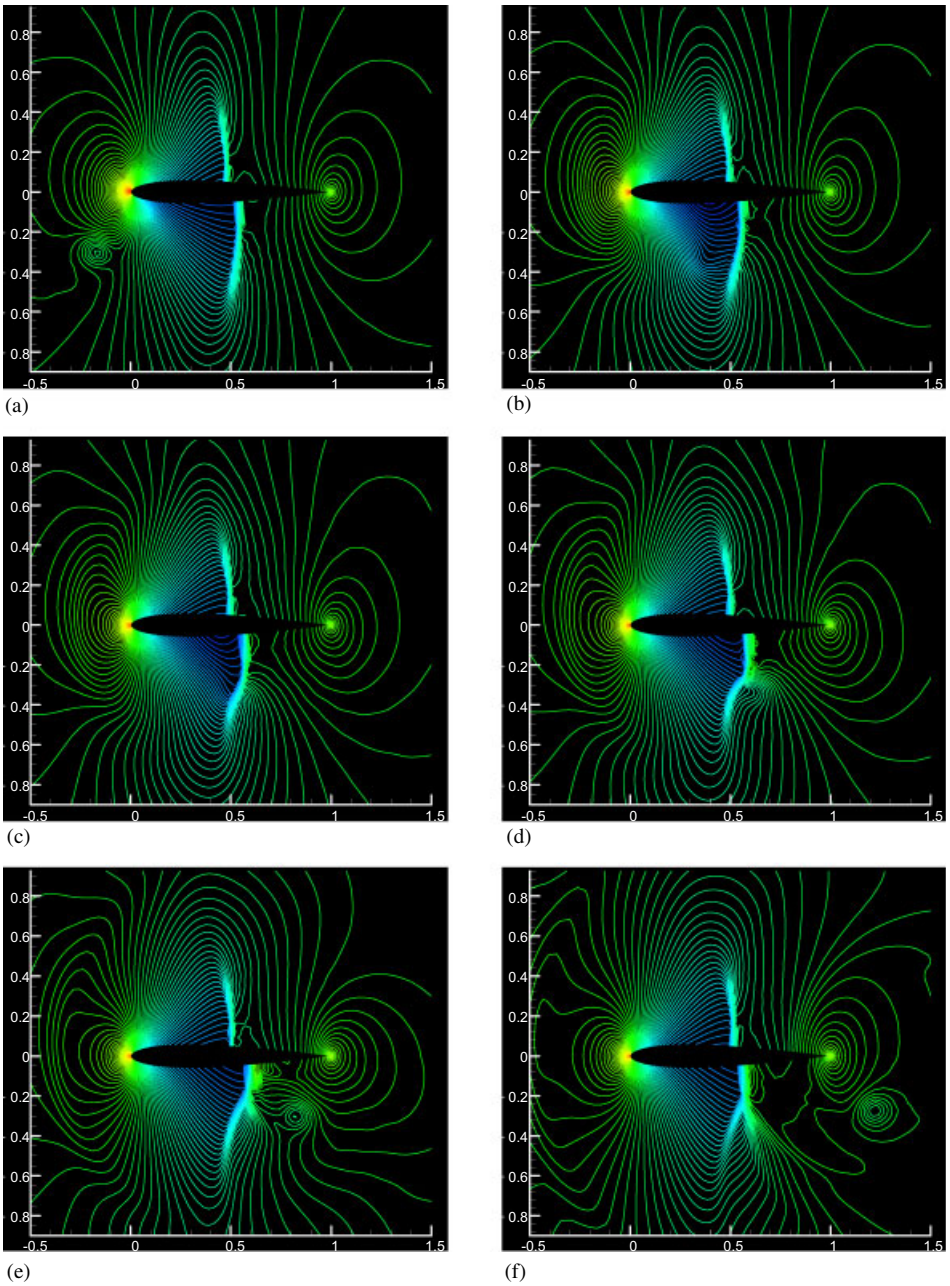

Figure 10. Instantaneous pressure contours for supercritical interaction: (a) $t=-0.1$; (b) $t=0.4$; (c) $t=0.5$; (d) $t=0.6$; (e) $t=0.8$; and (f) $t=1$ (Min $=0.3$, Max $=1.2$, Interval $=0.01$).

DOI: 10.1002/fld

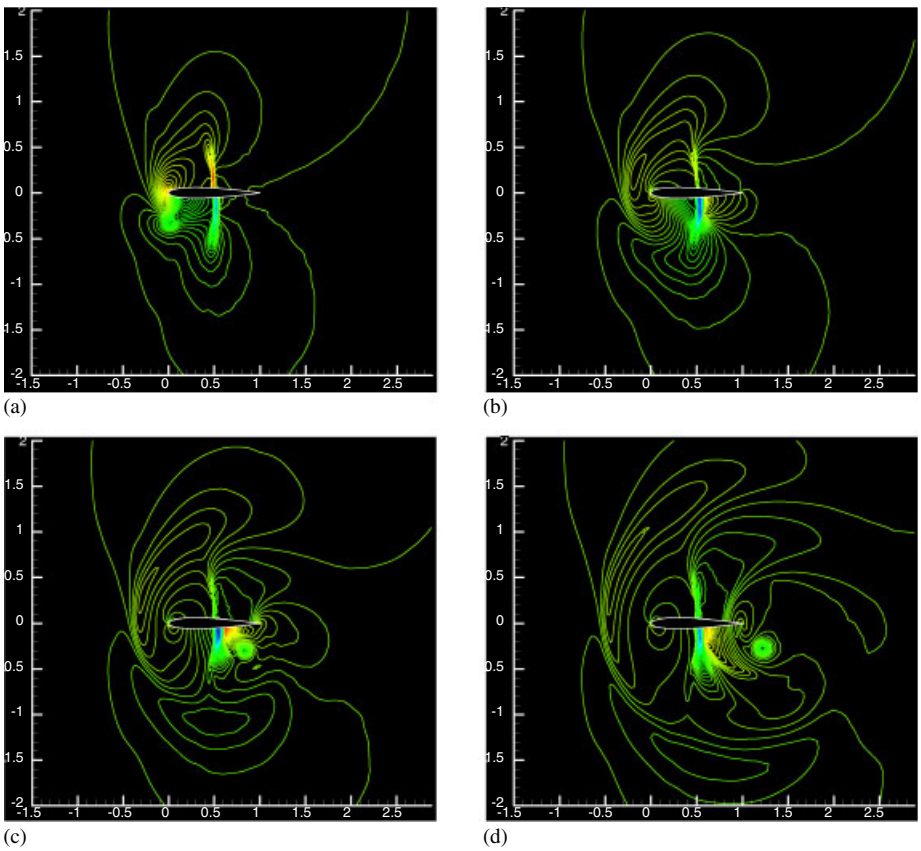

Figure 11. Perturbation pressure contours for supercritical interaction: (a) $t = 0.1$; (b) $t = 0.5$; (c) $t = 0.8$; and (d) $t = 1$ (Min $= -0.32$, Max $= 0.2$, Interval $= 0.0055$).

the vortex profiles given by the modified TURNS methodology are almost invariant. On the other hand, the one from the baseline TURNS methodology quickly evolves to a stabilized profile with only about 15% of the initial strength.

To check the shock deformation during the airfoil–vortex interaction, Figure 10 presents the instantaneous pressure contours predicted by the modified TURNS methodology when the vortex is 0.1 chord lengths upstream of the leading edge, and 0.4, 0.5, 0.6, 0.8, and 1 chord lengths downstream of the leading edge. It is found that until the vortex is 0.1 chord lengths upstream of the leading edge, the shock over the lower surface is still almost straight. As the vortex further approaches to this shock, the shock profile becomes curved. After the vortex passes by the shock, a lambda-type shock profile forms.

Figure 11 further presents the contours of the perturbation pressure, the subtraction of the initial undisturbed steady-state pressure from the instantaneous pressure, at four different time steps to illustrate the initial formation and propagation of the acoustic waves. Different from the subcritical case, the existence of the shocks over the upper and lower surfaces of the airfoil severely restricts the development of the negative perturbation pressure over the upper surface and

DOI: 10.1002/fld

the positive perturbation pressure over the lower surface after the induced angle of attack changes from negative to positive. In fact, the positive perturbation pressure pulse over the upper surface and the negative perturbation pressure pulse over the lower surface still attach to the airfoil after the vortex is well downstream of the airfoil. This explains why the loading in Figure 8 increases slowly after the shock–vortex interaction.

It is also found that besides accurately preserving the vortex structure, the modified TURNS methodology also captures much sharper acoustic wave fronts. This happens even when the grid redistribution is already turned off. To implement grid redistribution for improving acoustic wave capturing, one needs to use density gradient instead of the modified point attraction function of (1) to determine the length scale l in the grid redistribution method of Reference [19].

5. CONCLUSION

A grid redistribution method has been used together with an improved spatially third-order accurate Euler solver to achieve the accurate Euler simulations of airfoil–vortex interaction. The presented numerical results of two airfoil–vortex interaction cases indicate that with some extra works due to grid redistribution, the proposed approach is able to accurately preserve the vortex structure after a long convection and capture much sharper acoustic wave fronts without increasing the number of grid points. The approach can be straightforwardly extended for simulation of self-generated rotor blade–vortex interactions.

ACKNOWLEDGEMENTS

This work was initiated as the first author's PhD thesis work, which was partially supported by the National Rotorcraft Technology Center (NRTC) under the Rotorcraft Center of Excellence program. However, the majority of this work was done later under the support of NSF Grant DMI-0232255 to the first author. The authors would also like to acknowledge the reviewers for their valuable comments, especially the suggestion of the subcritical head-on interaction case.

REFERENCES

1. Srinivasan GR, McCroskey WJ, Baeder JD. Aerodynamics of two-dimensional blade–vortex interaction. *AIAA Journal* 1986; **24**:1569–1576.
2. Hassan AA, Tung C, Sankar LN. Euler solutions for self-generated rotor blade–vortex interactions. *International Journal for Numerical Methods in Fluids* 1992; **15**:427–451.
3. Parameshwaran P. Concepts for reduction of blade vortex interaction noise and the use of CFD to determine indicial and gust responses of an airfoil in compressible flow. *MS Scholarly Paper*, University of Maryland, 1995.
4. Steinhoff J, Raviprakash GK. Navier–Stokes computation of blade–vortex interaction using vorticity confinement. *AIAA-95-0161*, 1995.
5. Rai MM. Navier–Stokes simulation of blade–vortex interaction using high-order accurate upwind schemes. *AIAA-87-0543*, 1987.
6. Davoudzadeh F, McDonald H, Thompson BE. Accuracy evaluation of unsteady CFD numerical schemes by vortex preservation. *Computers and Fluids* 1995; **24**:883–895.
7. Wake BE, Choi D. Investigation of high-order upwinded differencing for vortex convection. *AIAA-95-1719*, 1995.
8. Jiang GS, Shu CW. Efficient implementation of weighted ENO scheme. *Journal of Computational Physics* 1996; **126**:202–228.
9. Suresh A, Huynh HT. Accurate monotonicity preserving scheme with Runge–Kutta time-stepping. *Journal of Computational Physics* 1997; **136**:83–99.

DOI: 10.1002/fld

10. Lele SK. Compact finite difference schemes with spectral-like resolution. *Journal of Computational Physics* 1992; **103**:16–42.
11. Tam CKW, Webb JC. Dispersion-relation-preserving finite difference schemes for computational acoustics. *Journal of Computational Physics* 1993; **107**:262–281.
12. Tang L, Baeder JD. Uniformly accurate finite difference schemes for *p*-refinement. *SIAM Journal on Scientific Computing* 1999; **20**:1115–1131.
13. Tang L. Improved Euler simulation of helicopter vortical flows. *Ph.D. Thesis*, University of Maryland, College Park, 1998.
14. Tang L, Baeder JD. Improving Godunov-type reconstructions for simulation of vortex dominated flows. *Journal of Computational Physics* 2006; **213**:659–675.
15. Ng NL, Hillier R. Numerical simulation of the transonic blade–vortex interaction. *Proceedings of the 22nd Annual European Rotorcraft Forum*, Brighton, U.K., 1996.
16. Hwang CJ, Kuo JY. Adaptive finite volume upwind approaches for aeroacoustic computations. *AIAA Journal* 1997; **35**:1286–1293.
17. Oh WS, Kim JS, Kwon OJ. Numerical simulation of two-dimensional blade–vortex interactions using unstructured adaptive meshes. *AIAA Journal* 2002; **40**:474–480.
18. Dannenhoffer III JF. A comparison of adaptive-grid redistribution and embedding for steady transonic flows. *International Journal for Numerical Methods in Engineering* 1991; **32**:653–663.
19. Tang L, Baeder JD. A two-step grid redistribution method. *Computers and Fluids* 2003; **32**:323–336.
20. Lee S, Bershader D. Head-on parallel blade–vortex interaction. *AIAA Journal* 1994; **32**:16–22.
21. Knupp PM. Jacobian-weighted elliptic grid generation. *SIAM Journal on Scientific Computing* 1996; **17**:1475–1490.
22. Srinivasan GR, Baeder JD, Obayashi S, McCroskey WJ. Flowfield of a lifting rotor in hover: a Navier–Stokes simulation. *AIAA Journal* 1992; **30**:2371–2378.
23. Thomas PD, Lombard CK. Geometric conservation law and its application to flow computations on moving grids. *AIAA Journal* 1979; **17**:1030–1037.
24. Vinokur M. An analysis of finite-difference and finite-volume formulations of conservation laws. *Journal of Computational Physics* 1989; **81**:1–52.

DOI: 10.1002/fld